Advances in Radiation Oncology (2021) 7, 100826

advances
in radiation oncology

www.advancesradonc.org

Scientific Article

Dosimetric Uncertainties in Dominant Intraprostatic Lesion Simultaneous Boost Using Intensity Modulated Proton Therapy

Jun Zhou, PhD,[a,*] Xiaofeng Yang, PhD,[a] Chih-Wei Chang, PhD,[a] Sibo Tian, MD,[a] Tonghe Wang, PhD,[a] Liyong Lin, PhD,[a] Yinan Wang, MS,[a] James Robert Janopaul-Naylor, MD,[a] Pretesh Patel, MD,[a] John D. Demoor, MS,[b] Duncan Bohannon, MS,[b] Alex Stanforth, MS,[a] Bree Eaton, MD,[a] Mark W. McDonald, MD,[a] Tian Liu, PhD,[a] and Sagar Anil Patel, MD[a]

[a]*Department of Radiation Oncology, Emory University, Atlanta, Georgia;* [b]*Department of Medical Physics, Georgia Institute of Technology, Atlanta, Georgia*

Received March 15, 2021; revised August 27, 2021; accepted September 20, 2021

Abstract

Purpose: While intensity modulated proton therapy can deliver simultaneous integrated boost (SIB) to the dominant intraprostatic lesion (DIL) with high precision, it is sensitive to anatomic changes. We investigated the dosimetric effects from these changes based on pretreatment cone-beam computed tomographic (CBCT) images and identified the most important factors using a multilayer perceptron neural network (MLPNN).

Methods and Materials: DILs were contoured based on coregistered multiparametric magnetic resonance images for 25 previously treated prostate cancer patients. SIB plans were created with (1) prostate clinical target volume − V70 Gy = 98%; (2) DIL − V98 Gy > 95%; and (3) all organs at risk (OARs) within clinical constraints. SIB plans were applied to daily CBCT-based deformed planning computed tomography (CT)**. DIL − V98 Gy, bladder/rectum maximum dose (Dmax) and volume changes, femur shifts, and the distance from DIL to organs at riskOARs in both planning computed tomogramsCT and CBCT were calculated. Wilcoxon signed-ranks tests were used to compare the changes. MLPNNs were used to model the change in ΔDIL − V98 Gy > 10% and bladder/rectum Dmax > 80 Gy, and the relative importance factors for the model were provided. The performances of the models were evaluated with receiver operating characteristic curves.**

Results: Comparing initial plan to the average from evaluation plans, respectively, DIL − V98 Gy was 89.3% ± 19.9% versus 86.2% ± 21.3% ($P = .151$); bladder Dmax 71.9 ± 0.6 Gy versus 74.5 ± 2.9 Gy ($P < .001$); and rectum Dmax 70.1 ± 2.4 Gy versus 74.9 ± 9.1Gy ($P = .007$). Bladder and rectal volumes were 99.6% ± 39.5% and 112.8% ± 27.2%, respectively, of their initial volume. The femur shift was 3.16 ± 2.52 mm. In the modeling of ΔDIL V98 Gy > 10%, DIL to rectum distance changes, DIL to bladder distance changes, and rectum volume changes ratio are the 3 most important factors. The areas under the receiver operating characteristic curves were 0.89, 1.00, and 0.99 for the modeling of ΔDIL − V98 Gy > 10%, and bladder and rectum Dmax > 80 Gy, respectively.

Sources of support: This work has no specific funding.
Disclosures: No conflict of interest for all authors.
Research data are not available at this time.
*Corresponding author: Jun Zhou, PhD; E-mail: jun.zhou@emory.edu

https://doi.org/10.1016/j.adro.2021.100826

Conclusions: Dosimetric changes in DIL SIB with intensity modulated proton therapy can be modeled and classified based on anatomic changes on pretreatment images by an MLPNN.

Introduction

Prostate cancer accounted for 20% of incident cancer cases in American men in 2019.[1] Radiation therapy (RT) is utilized in approximately half of the patients' treatments.[2] While the dose delivered to the prostate is typically homogeneous in external RT compared to brachytherapy, recent studies have shown that dose escalation to the dominant intraprostatic lesion (DIL), detected via multiparametric magnetic resonance imaging (MRI) scans,[3,4] could increase the tumor control probability.[5,6] Such dose escalation has been shown to be feasible with brachytherapy[3,7−12] and external beams using volumetric modulated arc therapy,[4,8,13−15] tomotherapy,[16] particle therapy,[9,17] and Cyberknife.[18]

Proton therapy provides superior dose distributions and dosimetric advantages over photon x-ray beams in many sites. Though the data supporting protons over intensity modulated RT for prostate cancer have been conflicting,[19,20] these studies predominantly included men treated with first-generation passive scattering proton therapy. The dosimetric advantages associated with advanced intensity modulated proton therapy (IMPT), as well as the application of online cone-beam computed tomographic (CBCT) image guidance, has the potential to reduce urinary/bowel toxicities by mitigating the volume of these structures receiving moderate-to-high doses. IMPT potentially will reduce radiation-induced secondary cancer for young patients.[21] Furthermore, with the advent of IMPT and CBCT image guidance, studies have shown the feasibility of using IMPT for DIL boost and perhaps the ability to further dose-escalate beyond that achievable with photons, thereby improving tumor control probability.[9,17,22]

Compared to photon therapy, however, proton therapy is more sensitive to the setup uncertainties and inter/intrafractional anatomy changes, such as rectum and bladder filling,[23] femur rotation, lateral tissue thickness variation, and so on.[24] Even with strict bladder filling protocol and rectum immobilization techniques, the uncertainties in prostate proton treatment are unavoidable. As the dose to the DIL is typically escalated to a much higher dose (from 120% to 200% of the prescription), any uncertainties in the patient setup and anatomy changes pose a significantly higher risk of overdose and subsequent toxicity to the critical organs in the close proximity.

In this study, we report the effect of various anatomic and setup uncertainties on DIL coverage and normal tissue avoidance in a cohort of men treated with IMPT. Secondly, we sought to identify predictors for DIL coverage and normal tissue avoidance changes that may be used to determine which patients can safely be treated with IMPT with dose escalation to DIL. A multilayer perceptron neural network (MLPNN) provided by commercial statistical analysis software was used to test the feasibility of modeling the DIL coverage drop and maximum dose to the bladder and rectum using critical parameters derived from the CBCT images and initial treatment plans. This work can be used for the prediction of treatment safety, the necessity of online adaptation,[25,26] and patient selection.

Materials and Methods

Patient selection and image acquisition

Twenty-five men with cT1-3bN0 prostate cancer undergoing IMPT to prostate ± proximal seminal vesicles with available first-week daily CBCT (total 125 CBCT images) were identified. The median age of the men was 69.5 years (range 49-83). Patients were scanned with 1.5 mm slice thickness at the simulation with a computed tomography (CT) scanner (Somatom Definition Edge, Siemens) for their planning CT (pCT) images. Immediately following CT simulation, each patient was scanned with a 1.5 T MRI scanner (Aera, Siemens) at the same setup position. T1, T2, and diffusion-weighted MRIs were acquired. Apparent diffusion coefficient maps were generated with b-value = 800 s/mm^2 for analysis.

Contouring and treatment planning

The clinical target volume (CTV) was outlined based on the MRI of the prostate and proximal seminal vesicles. DILs were contoured based on the multiparametric magnetic resonance images in Velocity AI 4.1 (Varian Medical Systems) with consensus from 2 radiation oncologists. The urethra was contoured on the MRI utilizing the T1 volumetric interpolated breath-hold sequence for each patient. Both DIL and urethra contours were rigidly transferred from MRIs to pCTs for treatment planning. The bladder, rectum, and femur head were contoured for each patient on their pCT images. Plans were created using opposed lateral beams, as shown in Figure 1. Robust optimization with 5 mm setup uncertainties in the anterior/posterior and superior/inferior directions combined with ±3.5% range uncertainties was used during the treatment planning. Simultaneous integrated boost (SIB) plans (prescription

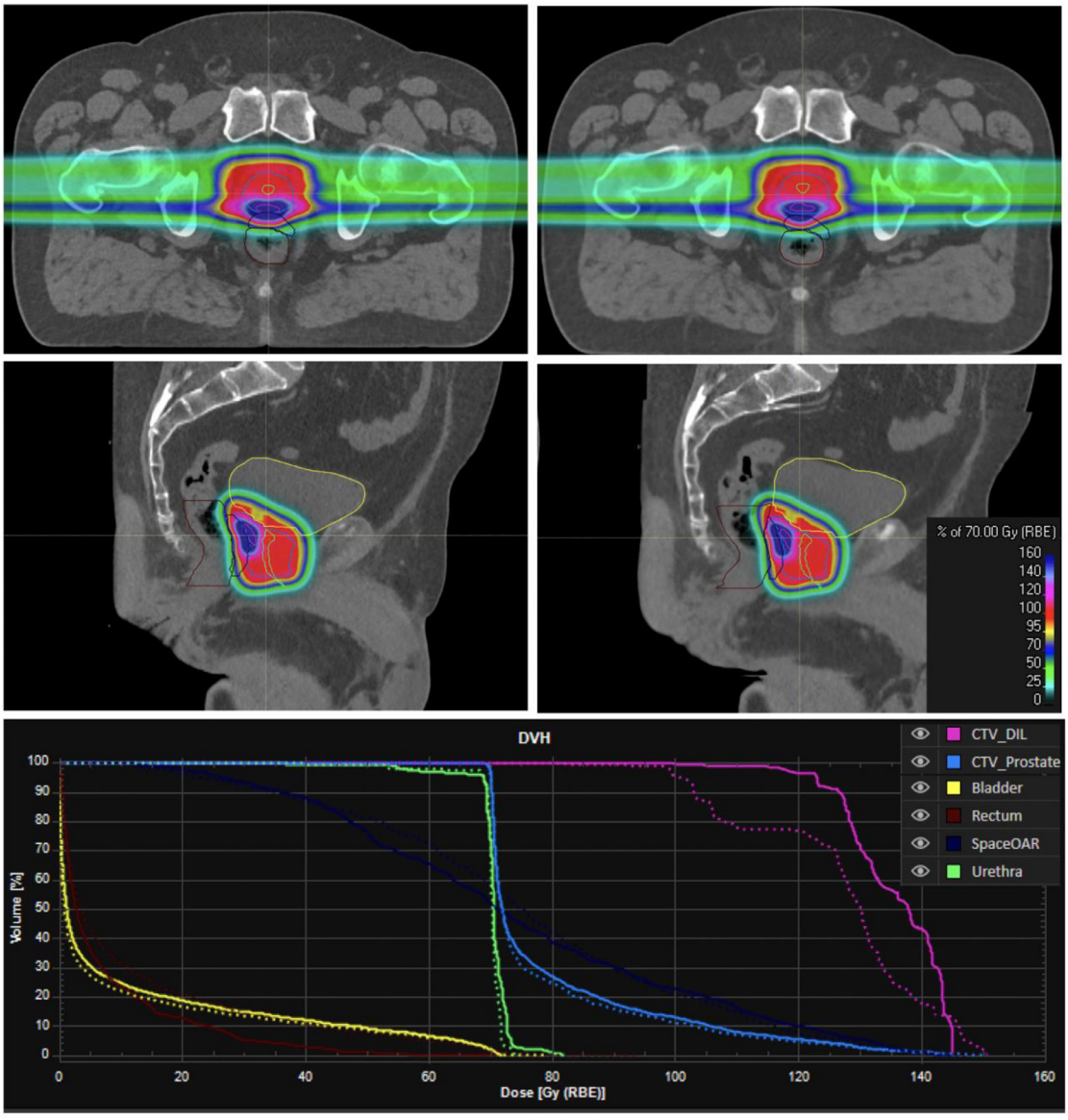

Figure 1 Axial (top) and coronal (middle) view of dose distribution of a prostate dominant intraprostatic lesion simultaneous integrated boost plan on the initial planning CT (left) and an evaluation deformed CT (right). The dose-volume histograms for the dominant intraprostatic lesion and prostate clinical target volume, bladder, rectum, and urethra in the initial plan (solid lines) and evaluation plan (dashed lines) are shown at the bottom. The contours in the deformed CT were drawn based on the cone-beam computed tomographic image. *Abbreviations:* CT = computerized tomogram.

70 Gy in 28 fractions) were created in RayStation 8B (RaySearch) so that (1) the CTV V100% normalized to 98% coverage; (2) DIL V98 Gy > 95% when possible; and (3) all organs at risk (OARs) constraints (Table 1) were met. A dose falloff objective was applied to the region surrounding the DIL so that the rest of the CTV was not overdosed. Both the CTV and the DIL were robustly optimized with high weightings. The CTV was covered with single field optimization (SFO) technique, while the DIL was optimized with multifield optimization (MFO) technique. While the overall maximum dose was limited at 145 Gy, the maximum dose to the "CTV − (DIL + 1.5 cm)" was robustly limited to 75 Gy.

Patient immobilization and setup

All patients were asked to drink 500 mL of water 1 hour before the simulation and each treatment. A rectal spacer (SpaceOAR Hydrogel, Augmenix, Inc.) was injected between the prostate and rectum. Three fiducial markers were implanted into the prostate before simulation CT for all patients. An empty rectum was advised for both simulation and treatments. All patients were treated in the supine position. Vacuum cushions were placed under the patients' knees to minimize the rotational variation of the femur bones.

Table 1 OAR dose constraints (RTOG 0415 arm 2[20])

CTV/OAR constraints	CTV	V100 = 98%
	Bladder	Dose to 15% (D15) ≤ 79 Gy
		D25 ≤ 74 Gy
		D35 ≤ 69 Gy
		D50 ≤ 64 Gy
	Rectum	D15 ≤ 74 Gy
		D25 ≤ 69 Gy
		D35 ≤ 64 Gy
		D50 ≤ 59 Gy
	Penile bulb	Mean ≤ 51 Gy
Optimizing goals	DIL	D95 ≥ 98 Gy when possible
		D90 ≥ 140 Gy as much as possible
	Bladder	Max < 71.5 Gy
	Rectum	Max < 71 Gy
	Femoral head	Max < 40 Gy
	Urethra	Max < 82 Gy

Abbreviations: CTV = clinical target volume; D = dose; DIL = dominant intraprostatic lesion; max = maximum; OAR = organ at risk.

At treatments, each patient was aligned to the bony structures with orthogonal kV images followed by CBCT imaging aligned to the fiducial markers. These online match registrations, which represented the treatment position, were saved and used for initial rigid registration between the CBCT and pCT during offline evaluation.

Quantification of anatomic variations and dosimetric changes

Figure 2 shows the workflow of the evaluation process. The pCT was deformed to the corresponding CBCT images in Velocity to create the deformed planning CT (dCT) for dose calculation. Though the image registration can successfully deform the body surface and bony structures, its accuracy on most soft tissue targets and OARs is not ideal. To evaluate the dosimetric parameters accurately, the prostate CTV, DIL, and urethra contours were rigidly copied to the CBCT (based on rigid registration of fiducial markers, assuming marker positions represent the prostate's position, and the DIL and urethra keep their relative position within prostate CTV), and then checked by a radiation oncologist and adjusted if needed. The bladder and rectum contours were recontoured in CBCT. As the rigid registrations were aligned to the fiducial markers, the femur head and bone structure may be misaligned. The mean deformation vector (femur deform) of the femoral heads was calculated from deformation matrix in Velocity. It is used as a parameter to predict the CTV coverage as the proton beam is sensitive to the water equivalent path length change along the beam. The level of dose escalation to the DIL as well the dose variation during daily treatment are mainly determined by its location relative to the critical structures. To quantify them, we calculated the shortest distance from the surface of the

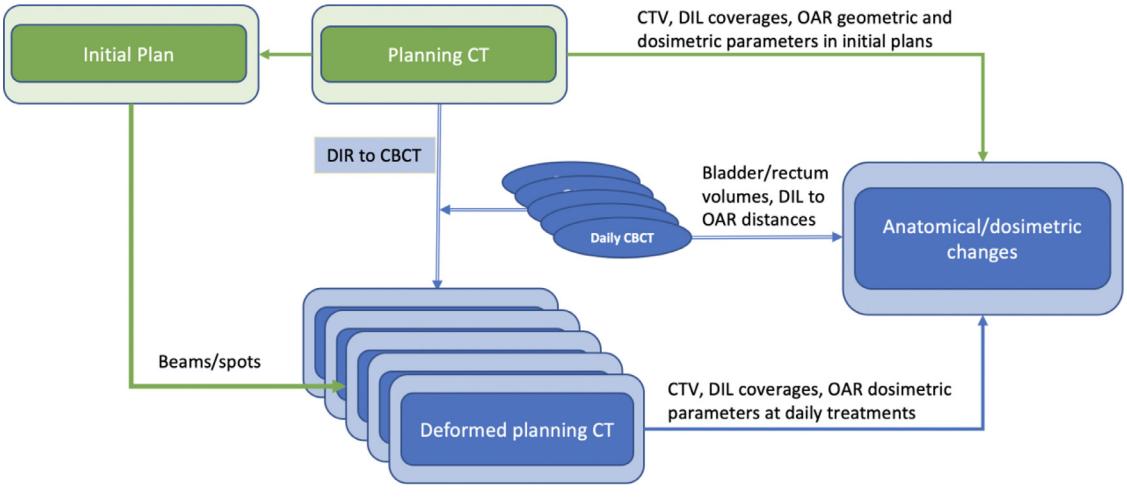

Figure 2 Flowchart of the evaluation process. *Abbreviations:* DIL = dominant intraprostatic lesion; DIR = deformable image registration; OAR = organ at risk.

DIL to the rectum (DIL to rectum) and bladder (DIL to bladder) in both pCT and CBCT images for each patient. The distances for DIL to urethra were calculated only on the pCT images.

The dCT images were sent to the planning system for dose calculations. Dosimetry parameters including CTV D99, DIL V98 Gy, and Dmax to the bladder and rectum were calculated for pCT and all daily dCT images.

As the anatomic/geometric and dosimetric parameters were not normally distributed, the Wilcoxon signed-rank test was used to compare the values at the simulation to those from daily treatments. Figure 1 demonstrates a DIL SIB plan on an initial planning CT and a dCT. The dose-volume histogram (DVH) differences for the dosimetry parameters are shown as well. The DIL dose in the evaluation changed substantially due to the enlarged rectum, though the DIL V98 Gy was barely changed.

Correlation of dosimetric changes with anatomic changes

To test the feasibility of modeling daily dosimetric changes, anatomic changes in daily CBCT images were calculated. These variables include bladder volume ratio and rectum volume ratio (ratio = volume in CBCT/volume in pCT), initial distance in pCT, actual distance in CBCT, and the corresponding changes from DIL to bladder and DIL to rectum, respectively (change = distance in CBCT − distance in pCT). A multivariate linear regression was used to find the predictors for initial DIL V98 Gy coverage. The dosimetric changes to the bladder, rectum, and DIL are complex and nonlinear functions of input variables. MLPNN modeling in SPSS version 26 (IBM) can identify the most important factors based on the quantity of normalized importance and were used to model bladder Dmax > 80 Gy, rectum Dmax > 80 Gy, and ΔDIL V98 Gy > 10%. The MLPNN consists of neurons interconnected with optimized weights. The neurons are simple nonlinear transfer functions that enable the MLPNN to approximate nonlinear functions. During the training process, the weights are determined in an iterative and back-propagation process to minimize the overall error of the model. The input layer includes all the variables mentioned previously (also shown in Supplementary Fig 1). Two hidden layers were used in the networks with 10 and 9 neurons in the first and second layer, respectively. Data from 125 treatment fractions were randomly chosen by the SPSS software, with 70% for training and 30% for testing. The process was run several times to check the modeling stability. The hyperbolic tangent and softmax activation functions are used for the hidden layers and the output layer, respectively. The normalized importance indexes for all the dosimetric and anatomic parameters are analyzed for each MLPNN model. The accuracy, defined as *(true positive prediction number + true negative prediction number)/total number* for either the training or the testing sets, of the models in the training and testing samples are presented. The performances of the models are further evaluated with receiver operating characteristic (ROC) curves. All statistical tests were conducted in SPSS statistics software with $P < .05$ deemed to be statistically significant.

Results

Mean CTV volume was 59.4 ± 27.9 cm^3 (range 24.1-131.0 cm^3). Mean bladder volume and rectum volume in daily CBCT vs pCT were 296.2 ± 153.6 cm^3 vs 299.3 ± 141.1 cm^3 (P =.757) and 53.5 ± 17.8 cm^3 vs 48.0 ± 16.2 cm^3 (P = .006), respectively (listed in Supplementary Table 1). The mean DIL to bladder distance and DIL to rectum distance in the CBCT vs pCT were 1.23 ± 0.84 cm vs 1.18 ± 0.81 cm (P = .042) and 1.81 ± 1.02 cm vs 1.84 ± 1.00 cm (P = .797), respectively. The mean DIL to urethra distance in pCT was 0.66 ± 0.43 cm. The mean volume ratios for the bladder and rectum were 99.6% ± 39.5% and 112.8% ± 27.2%, respectively. The mean femur deform was 3.16 ± 2.52 mm. The mean changes for DIL to bladder and DIL to rectum were 0.04 ± 0.01 cm and −0.04 ± 0.03 cm, respectively. Figure 3 shows the distributions of the bladder, rectum volume, and femur deform. The mean volume change ratio for bladder and rectum, the mean distance from DIL to the OARs, and their corresponding changes are also shown in Figure 3.

Dosimetric changes

The mean CTV D99% and DIL V98 Gy in dCT vs pCT were 69.6 ± 0.2 Gy vs 69.8 ± 0.1 Gy (P < .001) and 86.2% ± 21.3% vs 89.3% ± 19.9% (P = .151; Fig 4a-b), respectively (fraction dose was multiplied by the number of fractions to calculate the total dose). Mean bladder and rectum maximum dose in dCT vs pCT were 74.5 ± 2.9 Gy vs 71.9 ± 0.6 Gy (P < .001) and 74.9 ± 9.1 Gy vs 70.1 ± 2.4 Gy (P = .007; Fig 4e-f), respectively.

Correlation of dosimetric changes with anatomic changes

The linear model showed that the initial DIL to urethra distance (P < .01) is the prediction factor for initial DIL V98 Gy coverage. Figure 4c shows the frequency of DIL V98 Gy changes in percentage for all the CBCT evaluations. All the MLPNN models were stable. In the normalized importance of the MLPNN for the modeling of ΔDIL V98 Gy > 10%, DIL to rectum distance change, DIL to bladder distance change, and rectum volume change ratio

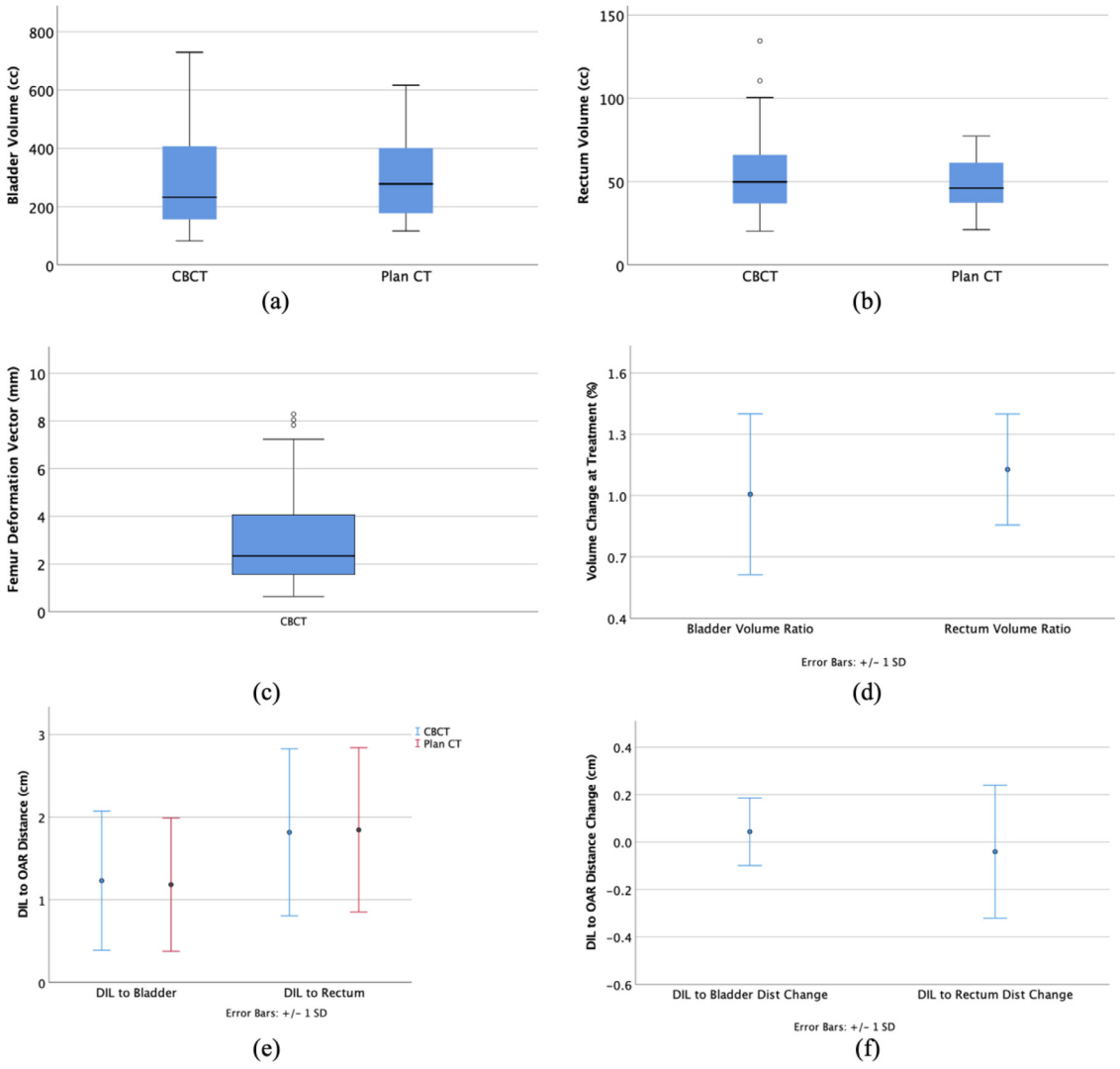

Figure 3 (a) Boxplot for bladder volume. (b) Boxplot for rectum volume. (c) Boxplot for the mean femur deformation vector. (d) Mean bladder and rectum volume ratio (= volume in cone-beam computed tomography/volume in planning computed tomography). (e) Mean distance from the dominant intraprostatic lesion to bladder and rectum. (f) Their corresponding changes at cone-beam computed tomography.

were the 3 most important factors (Fig 4d). The corresponding factors for bladder Dmax > 80 Gy were mean femur deformation vector, DIL to rectum distance change, and DIL to bladder distance change (Fig 4g). Rectum volume change ratio, DIL to bladder distance change, and initial DIL to rectum distance played the most important roles for rectum Dmax > 80 Gy in the dCT evaluations (Fig 4h).

In these 125 treatment fractions' data, there were 20, 10, and 16 records for ΔV98 > 10%, bladder Dmax > 80 Gy, and rectum Dmax > 80Gy, respectively. The accuracies of modeling ΔDIL V98 Gy > 10% were 84.7% and 83.5% in the training and testing samples, respectively. For the modeling of bladder Dmax > 80Gy, the accuracies were 100.0% and 94.9% in the training and testing samples, respectively. For the modeling of rectum Dmax > 80 Gy, they were 98.8% and 100.0%, respectively. The corresponding area under the receiver operating characteristic curves for each MLPNN model were 0.89, 1.00, and 0.99, respectively (Fig 5). The area under the curve (and the associated specificity and sensitivity) was calculated from combined training and testing samples.

Discussion

Studies have shown that the DIL is the most common site of recurrence after radiation therapy.[27,28] Many researchers have investigated the boost to DIL in clinical trials and demonstrated the safety of this treatment with brachytherapy, external beam x-ray radiation therapy (XRT), or combined therapy.[6,8,14,29] The SIB treatments with XRT alone show less escalated dose than those from brachytherapy (either mono or boost). The dosimetric

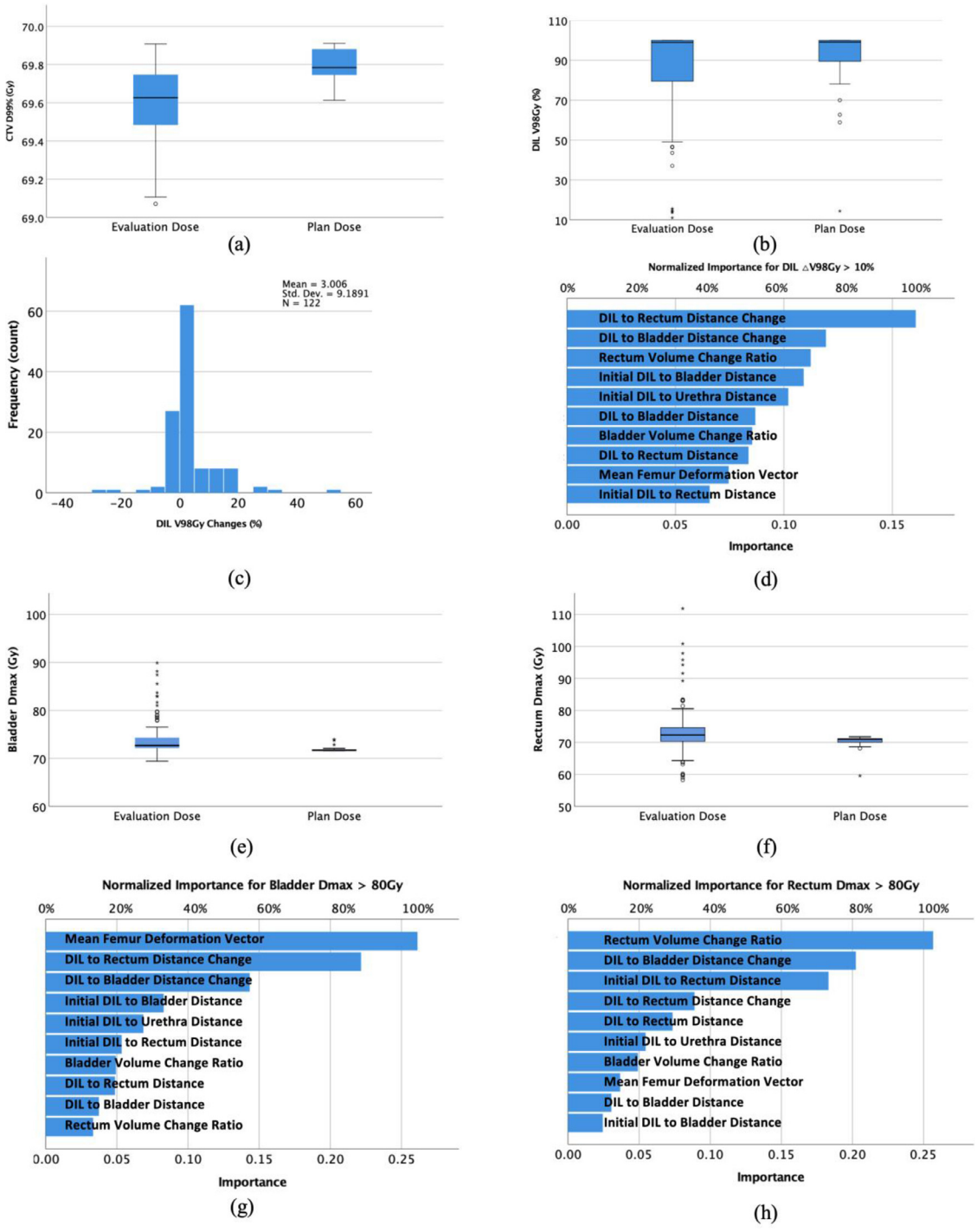

Figure 4 (a) Boxplot for clinical target volume D99 in evaluation plan and initial plans. (b) Boxplot for DIL V98 Gy in evaluation plan and initial plans. (c) Histogram of DIL V98 Gy changes for all evaluation fractions. (d) Normalized importance factors in the multilayer perceptron neural network for predicting change in DIL V98 Gy > 10%. (e) Boxplot of the bladder maximum doses in both the evaluation and the initial plans are shown at the bottom. (f) Boxplot of rectum maximum doses in both the evaluation and the initial plans are shown at the bottom. (g) Normalized importance factors for the bladder maximum dose > 80 Gy. (h) Normalized importance factors for the rectum maximum dose > 80 Gy. The stars and circles are outlier cases. *Abbreviations:* D = dose; DIL = dominant intraprostatic lesion.

uncertainties for XRT treating prostate without SIB technique have been extensively investigated.[23,24,30–35] However, the reports of uncertainty on SIB treatment are rare. Ballhausen et al reported a simulation study for the dosimetric impact from intrafraction motion on the DIL boost treatment using XRT and found that the DILs can be covered by 90% of SIB doses with 2 mm margin on them.[36]

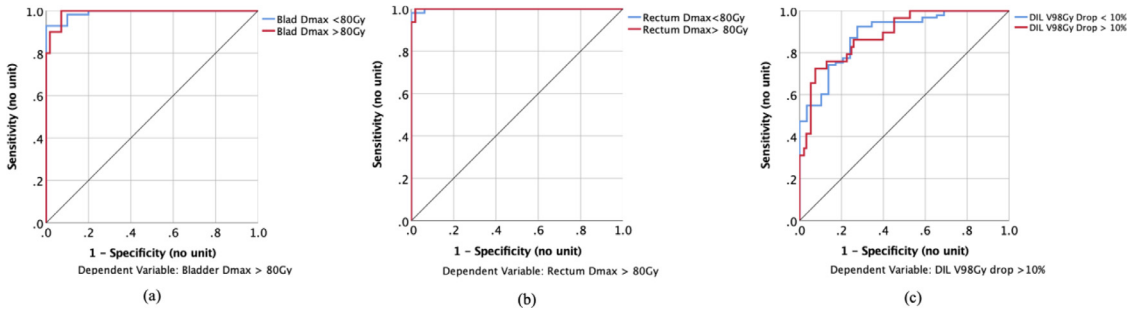

Figure 5 (a) Receiver operating characteristic curve for the modeling of bladder maximum dose > 80 Gy, using the multilayer perceptron neural networks. (b) Receiver operating characteristic curve for the modeling of rectum maximum dose > 80 Gy, using the multilayer perceptron neural networks. (c) Receiver operating characteristic curve for the modeling of change in dominant intraprostatic lesion V98 Gy > 10%, using the multilayer perceptron neural networks.

Advanced IMPT provides much better dosimetry than the XRT, thanks to the sharp distal falloff from the proton Bragg peak. However, IMPT is sensitive to range/setup uncertainties and anatomy changes. Studies have investigated the sensitivity of IMPT to interfraction uncertainty in proton therapy and found that rectal gas density overwrites and SFO are the 2 crucial factors for increasing the robustness of IMPT.[37] Park et al report that for prostate IMPT treatment, due to the variation in the rectal filling, rectum is the organ that is most sensitive to interfraction uncertainties. Rectum balloons have been used in many centers to address this issue.[38] Also, to reduce the dose to the rectum, a gel spacer has been inserted between the prostate and the rectum to reduce rectum dose.[39]

Most reports on dosimetric uncertainties in prostate proton therapy were using the nonboost technique with passive scattering proton therapy technique (in which it is difficult to implement high modulation and SIB boost to the DIL).[24,33,34,37] Some reports with the IMPT technique were using earlier proton pencil beam systems (larger spot size) without onboard CBCT capability.[30] Also, patient data were from previous photon treatment without strict bladder/rectum filling protocol and SpaceOAR techniques.

This study was based on prostate patients treated on a modern pencil beam scanning system with pretreatment CBCT image, implanted markers, and following imaging guided radiation therapy and bladder/rectum filling protocols. Although clear guidance was given to the patient regarding the bladder filling, the bladder volumes varied substantially among different patients (median 278 cm^3 and range 116 to 697 cm^3 at the simulation) and within each patient as well (standard deviations of bladder volumes in CBCT images varied from 14 to 492 cm^3 for the 25 patients). The variation at the simulation between patients was mostly due to the patients' anatomy differences, body hydration status at simulation, and the compliance with bladder filling protocol, while the variation at treatment was mostly due to the patients' compliance with the bladder filling protocol and uncertainty in actual treatment time slots. Though on average, the bladder volume at the simulation was similar to the corresponding volume at the treatments (P = .757; Supplementary Table 1), the maximum doses to the bladder at the treatments were significantly higher than their corresponding doses in the initial plans. The filled bladder can reduce the dose to the bladder and bowel. However, inconsistent bladder filling may result in the variation of prostate positions. It was found that bladder filling variation, resulting in changes from DIL to the bladder distance, plays one of the most significant factors that affect V98 Gy coverage (Fig 4e).

The rectum volume changes were greater than the bladder volume changes (Fig 3d). It was found that DIL to rectum distance change, resulting mainly from rectum filling variation, was one of the most significant factors to affect V98 Gy coverage (Fig 4d), bladder Dmax > 80 Gy (Fig 4g), and rectum Dmax > 80 Gy (Fig 4h). Rectum filling directly affects the prostate position relative to the femur head and body surface, which played a significant role in V98 Gy coverage reduction. Enema administration or rectal balloon can be used to reduce the uncertainty in rectum filling. Variation in rectum filling resulted in higher rectum Dmax (Fig 4h), which was sometimes systematically higher (patients 4, 7, and 23 in Supplementary Table 1).

The femur shift represented by femur deform partially resulted from bladder volume and rectum volume changes, and directly affected the DIL V98 Gy coverage, bladder Dmax, and rectum Dmax doses (Fig 4d-h).

The mean DIL to bladder distance was less than that to the rectum (Fig 3e), thanks to the implanted SpaceOAR, and possibly DIL tends to be closer to the prostate base and closer to the bladder. However, during treatments, the distances tended to increase for the DIL to the bladder, while they decreased for the DIL to the rectum (Fig 3f), which suggests a higher rectum maximum dose increase. As shown in Figure 3d-h, the DIL to rectum and bladder distance changes were the most important factors that affected the DIL coverage and the maximum doses to the bladder and rectum. The distances are much easier and faster to be measured online than the other anatomic

parameters, such as rectum and bladder volumes. They could be used as screening parameters to make quick decisions.

For DIL V98 Gy coverages there were wide variations between patients and fractions. Some initial coverages deviated from our goal (D95 > 98 Gy) due to the location of DIL relative to the OARs. Figure 4c shows the distribution of V98 Gy changes, of which the majority was within 10%. The top 3 factors in Figure 4d that affected the DIL V98 Gy coverages were all related to the rectum volume changes, which emphasizes the critical role of reducing the uncertainty of rectum filling. It also significantly affected the Dmax to the bladder and the rectum, as shown in Figure 4g-h.

Dmax doses to bladder and rectum were spread widely at the evaluation, shown in Figure 4e-f, which indicate the necessity of predicting their doses online. Linear models are difficult to model the Dmax changes for bladder and rectum, and the coverage changes to the DIL. The neural network, on the other hand, can model more accurately due to the ability to learn the representation in the training data and relate it to the output variables.

The neural network has been used for toxicity and outcome predictions.[40–43] In this study, we tested the feasibility of modeling dosimetric changes based on simple anatomy, geometry, and dosimetry paraments using commercial statistical analysis software (SPSS). The results show that it can accurately model the Dmax > 80 Gy for bladder and rectum. For DIL V98 Gy coverage, the accuracy is not ideal, partially due to the small size of DIL, high sensitivity of IMPT to the uncertainties, and heterogeneity of beam contributions from non-SFO plans.

One limitation of the study is that bilateral beam configurations were used unanimously for all plans. This beam arrangement can spare the bladder and rectum the most in most scenarios. In special situations like retreatment, more anterior and posterior oblique beams can be used to spread out the relative biological effectiveness uncertainties and increase the plan conformity (especially for stereotactic body radiation therapy (SBRT) cases).[44] In addition, uncertainties from intrafraction motion were not included in the study. Intrafraction bladder filling is continuous during the treatment and its effect can be reduced by adding interbeam kV imaging. Enema administration or rectum balloon can prevent intrafraction rectum filling uncertainties. Our study was based on 25 patients and 125 CBCT images from treatment fractions. More data are needed to improve the model's accuracy and robustness.

Conclusions

We have shown the effect of interfraction anatomy changes on the dosimetry of SIB to DIL using the IMPT technique. The importance factors for the dosimetric changes were investigated, and the feasibility of predicting OARs maximum dose and DIL coverage changes based on neural networks was demonstrated. To our knowledge, this is the first study of this kind on DIL boost using IMPT. It will provide information for clinical protocol design, treatment planning, online prediction, and patient selection. Patients with DIL near the urethra and bladder should be carefully evaluated before being enrolled in such treatments. Dosimetric parameters could be subject to anatomy changes, and an online dosimetric prediction tool is necessary for such treatment protocol. Future improvements include enlarging patient data, adding more patients' specific medical information into the model, etc. A more complicated model based on a deep convolution neural network can be used to improve the prediction performance.

Supplementary materials

Supplementary material associated with this article can be found in the online version at https://doi.org/10.1016/j.adro.2021.100826.

References

1. Rawla P. Epidemiology of prostate cancer. *World J Oncol*. 2019;10:63–89.
2. Barton MB, Jacob S, Shafiq J, et al. Estimating the demand for radiotherapy from the evidence: A review of changes from 2003 to 2012. *Radiother Oncol*. 2014;112:140–144.
3. Mason J, Al-Qaisieh B, Bownes P, et al. Multi-parametric MRI-guided focal tumor boost using HDR prostate brachytherapy: A feasibility study. *Brachytherapy*. 2014;13:137–145.
4. Alexander EJ, Murray JR, Morgan VA, et al. Validation of T2- and diffusion-weighted magnetic resonance imaging for mapping intraprostatic tumour prior to focal boost dose-escalation using intensity-modulated radiotherapy (IMRT). *Radiother Oncol*. 2019;141:181–187.
5. Kerkmeijer LGW, Groen VH, Pos FJ, et al. Focal boost to the intraprostatic tumor in external beam radiotherapy for patients with localized prostate cancer: Results from the FLAME randomized phase III trial. *J Clin Oncol*. 2021;39:787–796.
6. Monninkhof EM, van Loon JWL, van Vulpen M, et al. Standard whole prostate gland radiotherapy with and without lesion boost in prostate cancer: Toxicity in the FLAME randomized controlled trial. *Radiother Oncol*. 2018;127:74–80.
7. Wang T, Press RH, Giles M, et al. Multiparametric MRI-guided dose boost to dominant intraprostatic lesions in CT-based high-dose-rate prostate brachytherapy. *Br J Radiol*. 2019;92: 20190089.
8. Sanmamed N, Lee J, Berlin A, et al. Tumor-targeted dose escalation for localized prostate cancer using MR-guided HDR brachytherapy (HDR) or integrated VMAT (IB-VMAT) boost: Dosimetry, toxicity and health related quality of life. *Radiother Oncol*. 2020;149:240–245.
9. Andrzejewski P, Kuess P, Knäusl B, et al. Feasibility of dominant intraprostatic lesion boosting using advanced photon-, proton- or brachytherapy. *Radiother Oncol*. 2015;117:509–514.
10. Guimond E, Lavallée M-C, Foster W, et al. Impact of a dominant intraprostatic lesion (DIL) boost defined by sextant biopsy in permanent I-125 prostate implants on biochemical disease free survival (bDFS) and toxicity outcomes. *Radiother Oncol*. 2019;133:62–67.

11. Bauman G, Haider M, Van der Heide UA, et al. Boosting imaging defined dominant prostatic tumors: A systematic review. *Radiother Oncol*. 2013;107:274–281.
12. Kazi A, Godwin G, Simpson J, et al. MRS-guided HDR brachytherapy boost to the dominant intraprostatic lesion in high risk localised prostate cancer. *BMC Cancer*. 2010;10:472.
13. Zamboglou C, Thomann B, Koubar K, et al. Focal dose escalation for prostate cancer using 68Ga-HBED-CC PSMA PET/CT and MRI: A planning study based on histology reference. *Radiat Oncol*. 2018;13:81.
14. Murray JR, Tree AC, Alexander EJ, et al. Standard and hypofractionated dose escalation to intraprostatic tumor nodules in localized prostate cancer: Efficacy and toxicity in the DELINEATE trial. *Int J Radiat Oncol Biol Phys*. 2020;106:715–724.
15. den Hartogh MD, de Boer HCJ, de Groot-van Breugel EN, et al. Planning feasibility of extremely hypofractionated prostate radiotherapy on a 1.5 T magnetic resonance imaging guided linear accelerator. *Phys Imaging Radiat Oncol*. 2019;11:16–20.
16. Maggio A, Fiorino C, Mangili P, et al. Feasibility of safe ultra-high (EQD_2 >100 Gy) dose escalation on dominant intra-prostatic lesions (DILs) by helical tomotherapy. *Acta Oncol*. 2011;50:25–34.
17. Wang T, Zhou J, Tian S, et al. A planning study of focal dose escalations to multiparametric MRI-defined dominant intraprostatic lesions in prostate proton radiation therapy. *Br J Radiol*. 2020;93: 20190845.
18. Kim YJ, Yoon KJ, Kim YS. Simultaneous integrated boost with stereotactic radiotherapy for dominant intraprostatic lesion of localized prostate cancer: A dosimetric planning study. *Sci Rep*. 2020;10:14713.
19. Pan HY, Jiang J, Hoffman KE, et al. Comparative toxicities and cost of intensity-modulated radiotherapy, proton radiation, and stereotactic body radiotherapy among younger men with prostate cancer. *J Clin Oncol*. 2018;36:1823–1830.
20. Sheets NC, Goldin GH, Meyer A-M, et al. Intensity-modulated radiation therapy, proton therapy, or conformal radiation therapy and morbidity and disease control in localized prostate cancer. *JAMA*. 2012;307:1611–1620.
21. Vogel J, Lin L, Litzky LA, et al. Predicted rate of secondary malignancies following adjuvant proton versus photon radiation therapy for thymoma. *Int J Radiat Oncol Biol Phys*. 2017;99:427–433.
22. Moteabbed M, Harisinghani M, Efstathiou J, et al. Feasibility of ultrahigh dose escalations of MRI-defined intraprostatic lesions with proton therapy. *Presented at PTCOG 58*. Christie NHS, Manchester, United Kingdom; June 9-14, 2019.
23. Lin L, Vargas C, Hsi W, et al. Dosimetric uncertainty in prostate cancer proton radiotherapy. *Med Phys*. 2008;35:4800–4807.
24. Trofimov A, Nguyen PL, Efstathiou JA, et al. Interfractional variations in the setup of pelvic bony anatomy and soft tissue, and their implications on the delivery of proton therapy for localized prostate cancer. *Int J Radiat Oncol Biol Phys*. 2011;80:928–937.
25. Jagt T, Breedveld S, van Haveren R, et al. An automated planning strategy for near real-time adaptive proton therapy in prostate cancer. *Phys Med Biol*. 2018;63: 135017.
26. Jagt T, Breedveld S, van de Water S, et al. Near real-time automated dose restoration in IMPT to compensate for daily tissue density variations in prostate cancer. *Phys Med Biol*. 2017;62:4254–4272.
27. Pucar D, Hricak H, Shukla-Dave A, et al. Clinically significant prostate cancer local recurrence after radiation therapy occurs at the site of primary tumor: Magnetic resonance imaging and step-section pathology evidence. *Int J Radiat Oncol Biol Phys*. 2007;69:62–69.
28. Arrayeh E, Westphalen AC, Kurhanewicz J, et al. Does local recurrence of prostate cancer after radiation therapy occur at the site of primary tumor? Results of a longitudinal MRI and MRSI study. *Int J Radiat Oncol Biol Phys*. 2012;82:e787–e793.
29. von Eyben FE, Kiljunen T, Kangasmaki A, et al. Radiotherapy boost for the dominant intraprostatic cancer lesion—a systematic review and meta-analysis. *Clin Genitourin Cancer*. 2016;14:189–197.
30. Soukup M, Söhn M, Yan D, et al. Study of robustness of IMPT and IMRT for prostate cancer against organ movement. *Int J Radiat Oncol Biol Phys*. 2009;75:941–949.
31. Park PC, Cheung JP, Zhu XR, et al. Statistical assessment of proton treatment plans under setup and range uncertainties. *Int J Radiat Oncol Biol Phys*. 2013;86:1007–1013.
32. Moteabbed M, Trofimov A, Sharp GC, et al. Proton therapy of prostate cancer by anterior-oblique beams: Implications of setup and anatomy variations. *Phys Med Biol*. 2017;62:1644–1660.
33. Maeda Y, Sato Y, Minami H, et al. Positioning accuracy and daily dose assessment for prostate cancer treatment using in-room CT image guidance at a proton therapy facility. *Med Phys*. 2018;45:1832–1843.
34. Su Z, Slopsema R, Flampouri S, et al. Impact of intrafraction prostate motion on clinical target coverage in proton therapy: A simulation study of dosimetric differences in two delivery techniques. *J Appl Clin Med Phys*. 2019;20:67–73.
35. Andersen AG, Casares-Magaz O, Muren LP, et al. A method for evaluation of proton plan robustness towards inter-fractional motion applied to pelvic lymph node irradiation. *Acta Oncol*. 2015;54:1643–1650.
36. Ballhausen H, Li M, Reiner M, et al. Dosimetric impact of intrafraction motion on boosts on intraprostatic lesions: A simulation based on actual motion data from real time ultrasound tracking. *Radiat Oncol*. 2019;14:81.
37. Moteabbed M, Trofimov A, Sharp GC, et al. A prospective comparison of the effects of interfractional variations on proton therapy and intensity modulated radiation therapy for prostate cancer. *Int J Radiat Oncol Biol Phys*. 2016;95:444–453.
38. Su Z, Zhao T, Li Z, et al. Reduction of prostate intrafraction motion using gas-release rectal balloons. *Med Phys*. 2012;39:5869–5873.
39. Rucinski A, Brons S, Richter D, et al. Ion therapy of prostate cancer: Daily rectal dose reduction by application of spacer gel. *Radiat Oncol*. 2015;10:56.
40. Ibragimov B, Toesca D, Chang D, et al. Development of deep neural network for individualized hepatobiliary toxicity prediction after liver SBRT. *Med Phys*. 2018;45:4763–4774.
41. Buettner F, Gulliford SL, Webb S, et al. Using dose-surface maps to predict radiation-induced rectal bleeding: A neural network approach. *Phys Med Biol*. 2009;54:5139–5153.
42. Ibragimov B, Toesca DAS, Yuan Y, et al. Neural networks for deep radiotherapy dose analysis and prediction of liver SBRT outcomes. *IEEE J Biomed Health Inform*. 2019;23:1821–1833.
43. Liang B, Tian Y, Chen X, et al. Prediction of radiation pneumonitis with dose distribution: A convolutional neural network (CNN) based model. *Front Oncol*. 2020;9:1500.
44. Draulans C, De Roover R, van der Heide UA, et al. Stereotactic body radiation therapy with optional focal lesion ablative microboost in prostate cancer: Topical review and multicenter consensus. *Radiother Oncol*. 2019;140:131–142.